Dielectric and thermal properties of cerium dioxide up to 1000 degrees C and the effect of the porosity for microwave processing studies

Hussein Hammoud, S. Vaucher, François Valdivieso

Dielectric and thermal properties of cerium dioxide up to 1000 °C and the effect of the porosity for microwave processing studies

Hussein Hammoud[a,b,*], Sébastien Vaucher [a], Franc¸ois Valdivieso [b]

[a] *Swiss Federal Laboratories for Materials Science and Technology (EMPA), Thun, Switzerland*
[b] *Laboratoire Georges Friedel CNRS UMR 5307, St-Etienne, France*

This work presents the experimental determination of the thermal and dielectric properties of conventionally sintered cerium dioxide (CeO_2) samples, with a porosity ranging from 3.68 up to 44.33 vol%. The thermal conductivity, the thermal diffusivity and the heat capacity is determined using Laser Flash analysis and Differential Scanning Calorimetry. A cylindrical microwave cavity was developed to measure dielectric properties up to 1000 °C. The real and imaginary parts of the relative dielectric permittivity; ε'_r and ε''_r the dielectric loss factor, are obtained using the cavity perturbation theory in TM_{012} mode at 2.45 GHz. These parameters can be used as inputs for coupled thermo-mechano-electromagnetic modelling of Ceria sintering.

1. Introduction

The microwaves field has a variety of applications, from the wireless communication technologies to areas of materials processing, such as curing of wood, cooking food, filters, tempering, resonators, biomedical fields . . .. Microwaves are also used in national security applications, such as early warning radar, Doppler radars and the remote sensing technique for detecting the weather changes [1–4].

Microwave processing in materials, which includes the heating and the sintering, is quite different from the conventional one. In conventional furnaces, the heat is transferred from the source to the sample surface from where it then diffuses towards the sample core. The heat transfer process from the surface to the core of the sample is generally slow and results in high energy consumption [5]. Microwaves however are able to penetrate deeper inside the sample before their electromagnetic energy is converted into thermal energy. This heating can be rapid, "volumetric", homogeneous but remains dictated by the properties of the materials. Hence, it is essential and necessary to unravel the complex permittivity and the thermal conductivity for each material to be processed. Nowadays, microwave technology is helping to improve the sintering process for numerous materials [6]. Sintering based on microwave heating is claimed to be more advantageous than conventional sintering due to faster heating, lower sintering temperatures, improved physical and mechanical properties and other unique properties which are not observed in conventional processes [7]. During sintering by conventional heating, the flow of matter through grain boundaries or interfaces is required for both densification and grain growth. However, the detailed mechanisms involved during microwave heating remain unclear at this time and it could be that densification by microwave heating would be enhanced by specific sintering mechanisms such as field enhanced diffusion.

Cerium dioxide (ceria) has outstanding properties such as optical transparency, high refractive index and high dielectric constant, which make it suitable for various applications [8]. CeO_2 belongs to the family of fluorites [9], maintaining a cubic fluorite-type structure stable from room temperature up to its melting point (2700 °C) [10].

Ceria is used in a variety of applications such as polishing agent, UV filter (especially against skin cancer), oxygen storage material and as catalyst. In the research on nuclear fuels, ceria is used as non-radioactive simulant for plutonium [11], for example in the development of SpherPac fuel.

A previous study [12] allowed the synthesis of millimetric sphere-shaped CeO_2 xerogel particles by microwave assisted internal gelation. The porous spheres obtained must be further densified by sintering.

* Corresponding author at: Laboratoire Georges Friedel CNRS UMR 5307, 158 Cours Fauriel, 42023 Saint Etienne, France. Tel.: +33 477420002.
E-mail address: hammoud@emse.fr (H. Hammoud).

This study aims at evaluating the potential of microwave assisted densification of a cerium oxide xerogel towards a fully dense ceria. The first step is to determine the variation of the dielectric properties and the thermal conductivity of porous cerium oxide (density 55–96%) as function of temperature and densification. This should clarify the effect of microstructure changes by gradual porosity resorption during sintering on the microwave absorption.

Porous ceria is taken as a heterogeneous mixture of air and solid particles. Hence, a mixing rule is needed to express the effective thermo-physical parameters of the mixture in terms of the volume fraction of its components and their properties.

1.1. Effective permittivity

The effective permittivity in this case depends strongly on the content, and can be well presented by using the Maxwell-Garnet [13] model given in Eq. (1). It is based on the polarization induced by an external electric field in a medium where spherical inclusions were dispersed.

$$\frac{\varepsilon_{\text{eff}} - \varepsilon_s}{\varepsilon_{\text{eff}} + 2\varepsilon_s} = p\frac{\varepsilon_i - \varepsilon_s}{\varepsilon_i + 2\varepsilon_s} \tag{1}$$

This relationship can be rearranged:

$$\varepsilon_{\text{eff}} = \varepsilon_s \frac{1 + 2\chi}{1 - \chi} \tag{2}$$

With $\chi = p\frac{\varepsilon_i - \varepsilon_s}{\varepsilon_i + 2\varepsilon_s}$ where ε_s is the permittivity of the solid particles (cerium dioxide), ε_i is the permittivity of the spherical inclusions (air), ε_{eff} is the effective permittivity of the medium and p is the volume fraction of the spherical inclusions. In our case, the medium was ceria and inclusions were considered as air gas. Because the permittivity has a complex form with a real and imaginary parts ($\varepsilon = \varepsilon' - i \cdot \varepsilon''$) both values are considered evolving as Eq. (2). This is the simplest model and we should keep in mind that it overlooks the effect of the size of the pores and the size of the particles.

1.2. Effective thermal conductivity

For the composite materials or the materials which have many phases, the thermal conductivity depends widely on the volume fraction, the type of the phases, the geometry of the pores, their distribution and the influence of the grain boundaries [14].

Here, we present some models which were found to correlate well the thermal conductivity of such porous ceramics materials.

Francl et al. [15] suggested the following equation (Eq. (3)) for ceramics materials having isometric and anisometric pores randomly arranged:

$$\frac{\lambda}{\lambda_0} = 1 - p \tag{3}$$

where λ and λ_0 are, respectively, the thermal conductivity of a porous ceramic materials and the full dense ceramic material and p is the volume pore fraction.

On the basis of the Odelevskii equations, Aivazov and Domashnev [16] obtained the following Eq. (4) to represent the thermal conductivity of porous titanium nitride. In this case, they suggest a factor m to represent the pore distribution and the pore shape in the specimens.

$$\frac{\lambda}{\lambda_0} = \frac{1 - p}{1 + m \cdot p} \tag{4}$$

where m is a linear function of porosity (Eq. (5)) for $m \geq 0$.

$$m = a \cdot p \tag{5}$$

After substituting into Eq. (4), it results the following equation:

$$\frac{\lambda}{\lambda_0} = \frac{1 - p}{1 + a \cdot p^2} \tag{6}$$

where $a \geq 0$, this value was found equal to 6 for titanium nitride, and 10 for polycrystalline graphite [17].

Maxwell considered a matrix of materials made of spheres which are enough small that do not interact thermally with the continuous solid phase [18]. Therefore, he proposed for low volume fraction of porosity p:

$$\frac{\lambda}{\lambda_0} = 1 + \frac{3 \cdot p}{\left(\lambda_1 + 2 \cdot \lambda_0/\lambda_1 - \lambda_0\right) - p} \tag{7}$$

where λ_1 is the thermal conductivity of the inclusions, in our case we take the value 0 for the air. Therefore, Eq. (7) can be transformed in the following equation:

$$\frac{\lambda}{\lambda_0} = 1 - \frac{3 \cdot p}{2 + p} \tag{8}$$

Moreover, Rayleigh suggested a model for large volume fraction where the interaction between the spheres is small and the position of it is at the intersections of a cubic lattice [19].

After substituting the value of the air thermal conductivity directly we obtain

$$\frac{\lambda}{\lambda_0} = 1 - \frac{3 \cdot p}{2 + p - 0.39225p^{10/3} + \cdots} \tag{9}$$

As the interaction of the spheres is usually neglected, the model of Maxwell is still better and simpler.

However, for non-spherical inclusions, Maxwell's equation was modified in order to show the contribution of the thermal conductivity tensor. In case of long cylinder porosity parallel to z-axis, this tensor is composed by three components, the one which is parallel to z-axis is given by Eq. (3) and the other two components for x- and y-axis, supposed equals, are given by the following equation:

$$\frac{\lambda_{xx}}{\lambda_0} = \frac{\lambda_{yy}}{\lambda_0} = 1 - \frac{2.p}{1 + p + \left(0.30584.p^4 + 0.013363.p^8 + \ldots\right)} \tag{10}$$

Also, for complex inclusions, in case of unconsolidated granular beds, Eq. (11) allows a good relationship between conductivity and porosity [20,21]:

$$\frac{\lambda}{\lambda_0} = \frac{(1 - p)}{1 + (\alpha - 1).p} \tag{11}$$

in which α includes a shape factors.

$$\alpha = \frac{1}{3}\sum_{i=1}^{3}[1 - g_i]^{-1} \tag{12}$$

The shape factors g_i satisfy the relation $g_1 + g_2 + g_3 = 1$ and are equal to 1/3 for spheres. Then, in our case $\alpha = 1.5$ for spherical inclusions and the equation is simplified to Eq. (8). These several models show the variety of interaction possible between the porosity and the thermal conductivity: pore content and pore shape seem to be the most important parameters.

2. Materials and methods

2.1. Preparation of ceria pellets

A commercial powder of cerium dioxide (CER (IV)-OXID 99.9%, Aldrich,), with a particle size less than 5 μm, and with theoretical density 7.13 g/cm^3 was used. Pellets were pressed uniaxially in a tungsten carbide die with 12 mm diameter with different values of pressure (Table 1). The height of the green samples was fixed to 2 mm for thermal analysis and 18 mm for dielectric measurements.

Table 1
Series of samples with their forming conditions and final densities.

Serial number	Pressure (MPa)	Sintering temperature (°C)	Dwell time (h)	Density (%) of samples for the measurement of thermal properties	Density (%) of samples for the measurement of the dielectric properties	Standard deviation (%)
1 (4 samples)	30	1050	4	55.67	56.59	0.48
2 (4 samples)	50	1250	0	59.29	62.40	1.46
3 (4 samples)	50	1400	0	65.50	66.87	0.67
4 (3 samples)	50	1500	0	73.63	–	1.75
5 (4 samples)	50	1500	1	–	87.42	2.48
6 (5 samples)	50	1500	3	89.92	90.27	2.25
7 (4 samples)	300	1600	3	96.32	95.48	0.41

The pellets were heated in air at 5 °C/min up to sintering temperature (1050, 1250, 1500 and 1600 °C) which were maintained for various dwell time (0, 1, 3 and 4 h) in order to cover a porosity range from 3.68 up to 44.33 vol%. For each series three to five samples were prepared (see Table 1), only one of them was used for thermal properties measurement. The porosity was determined using Archimedes' method.

Microstructure of four specimens were observed by SEM (JSM-6400) after cutting samples according perpendicular and parallel planes to the pressure axis and several polishing steps up to a final one of 1 μm were made.

2.2. Thermal conductivity measurement

The thermal conductivity λ was determined indirectly by measuring the thermal diffusivity α in argon using the Laser Flash Analysis (LFA 457 Microflash, Netzsch, Germany) [22], and the specific heat c_p, by using a Differential Scanning Analysis (DSC 404C, Netzsch, Germany). Then, the thermal conductivity λ was calculated using the following equation:

$$\lambda = \alpha\, \rho\, c_p \tag{13}$$

where ρ is the density (kg/m^3); c_p is the specific heat capacity (J/kg/K); α is the thermal diffusivity (m^2/s).

The thermal diffusivity was determined from five measurements at each temperature for each sample. The diffusivity was measured under argon flow (50 ml/min) from room temperature up to 1000 °C (100 °C by step). Using a low amount of Ceria powder (187.3 mg) the heat capacity was determined in the same gas flow condition as in LFA, with 15 °C/min heating rate. The uncertainty of DSC method is less than 1% [23].

2.3. Dielectric properties measurement

The samples were placed in a quartz crucible (9.7 mm $\text{diam}_{\text{in}} \times 12$ mm $\text{diam}_{\text{out}} \times 60$ mm long) and inserted in a quartz tube (13 mm $\text{diam}_{\text{in}} \times 15$ mm $\text{diam}_{\text{out}} \times 600$ mm long) (Fig. 1). The quartz tube was introduced in a vertical cylindrical conventional furnace (Superthal Mini, MS 26, Kanthal, Sweden) and the sample was heated in 50 °C steps. A waiting time of 10 min at each temperature step was imposed before the sample was moved into the resonant microwave cavity.

The microwave resonator was a water cooled vertical cylindrical aluminum cavity (42.5 mm $\text{radius}_{\text{in}} \times 17$ mm height) with two openings diam_{in} 17 mm to let the quartz tube through along the axis. The complex scattering parameters were determined from the measurement of the reflection coefficient (S11) using a Vector Network Analyzer (VNA, 8720D Agilent/HP, Calibration is carried out before the measurement [24]). The shift of the resonant frequency and the change in quality factor were extracted from the measured *S*-parameters based on a method proposed by Kajfez [25]. The cavity perturbation theory associated to the mode TM_{012} was used to determine the dielectric constant ε_r and the loss factor ε_r''. The mathematical model of the calculation is given in the following equations [26]:

$$\frac{f_0 - f_s}{f_0} = \left(\varepsilon_r' - 1\right) \cdot A \cdot B \cdot G \cdot \frac{V_s}{V_c} \tag{14}$$

$$\frac{1}{Q_s} - \frac{1}{Q_0} = 2\varepsilon_r'' \cdot A \cdot B \cdot G \cdot \frac{V_s}{V_c} \tag{15}$$

where f_0, f_s, Q_0, Q_s are, respectively, the resonance frequency and the quality factor of the TM012 mode of the cavity without and with sample. The *A*, *B* and *G* coefficients depend on the cylindrical Bessel functions and the dimensions of the cavity and the sample [27].(16)$A = J_0^2\left(2.405\frac{R_s}{R_c}\right) + J_1^2\left(2.405\frac{R_s}{R_c}\right)$

$$B = 1 + \left[\frac{L}{2\pi.H_s}\right] \cdot \sin\left(\frac{2\pi \cdot H_s}{L}\right. \quad \cdot \cos\left(\frac{4\pi \cdot H_c}{H_s}\right. \tag{17}$$

And

$$G = (0.2178).\left(\frac{c_0}{f_0.R_c}\right. \tag{18}$$

where H_c, R_c, V_c, H_s, R_s, V_s are, respectively, the length, the radius and the volume of the cavity without and with the sample. ***L*** is the length of coupling which is 3 mm in our case. Q_0 of the cavity varies between 1400 and 1500 depending on the initial conditions of the measurement (the initial temperature of the cavity and the calibration of the VNA). The temperature of the furnace was measured using a thermocouple (Fig. 1).

Finally, the dielectric loss tangent is given by the following equation:

$$\tan\delta = \frac{\varepsilon_r''}{\varepsilon_r'} \tag{19}$$

The measurement error using the swept-frequency method is less than ±5% for ε_r' and ±15% for ε_r'' [25]. This measurement accuracy is limited by the existence of convection phenomena of air at high temperature during the measurement stage.

3. Results

3.1. Microstructure for porous and dense materials

The characterization was made on the cross section parallel to applied pressure axis and on the surface which is perpendicular to it. The results for both kinds of planes were similar: No differences of pore fraction and pore shape were identified. In Fig. 2, four examples of microstructures observed for sintered samples only for perpendicular surfaces to the pressing axis are shown.

After heat treatment at 1250 °C (Fig. 2a) very low shrinkage was observed after sintering, and porosity (59.29%td) has an irregular shape, while homogenously distributed and interconnected. For a higher densification (1500 °C; 73.63%td), porosity remains interconnected; while its contours are smoothed (Fig. 2b). For higher densification (82.63%td), it appears some non-homogenous densification, indeed some zones appear denser with closed porosity

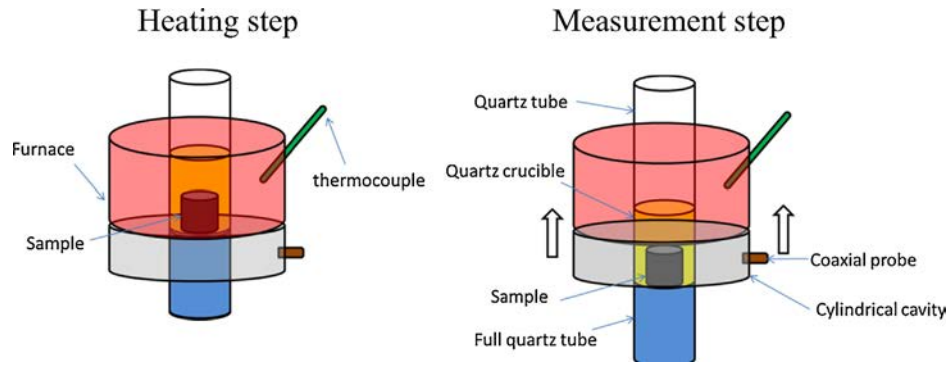

Fig. 1. Schematic shows the developed system for the dielectric measurement.

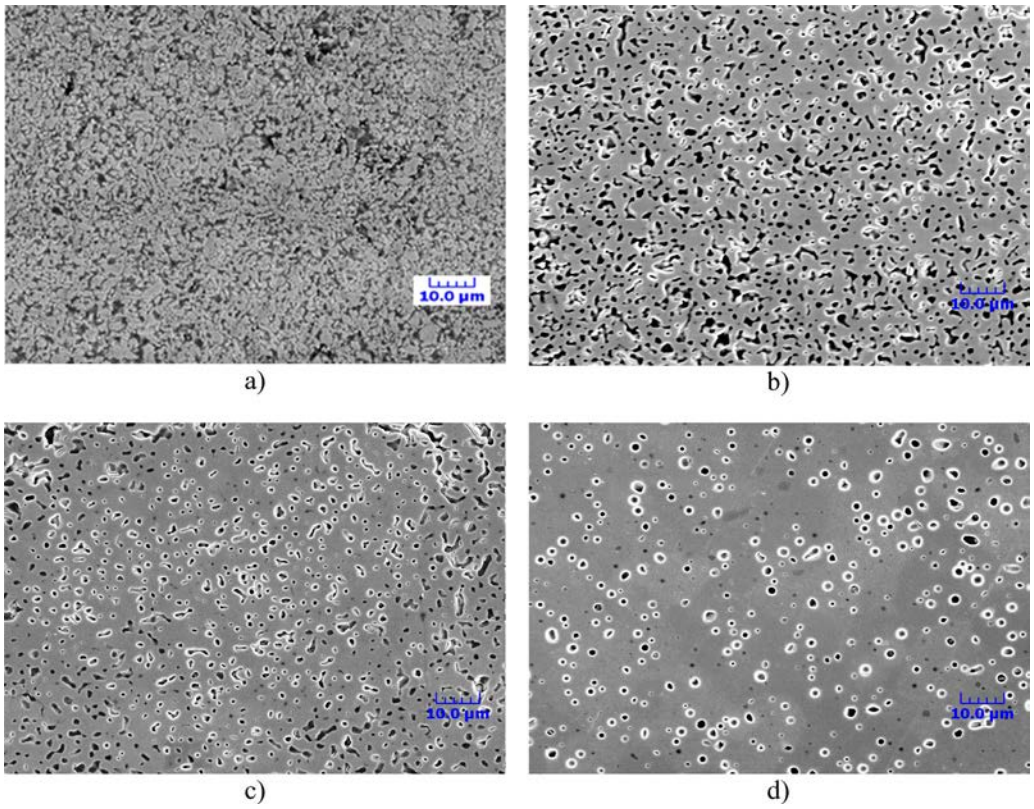

Fig. 2. SEM micrographs showing four samples: (a) 59.29%, (b) 73.63%, (c) 82.63%, (d) 89.92%.

surrounded by zones with higher porosity ratio but in which porosity stays open (Fig. 2c). And finally, close to the theoretical density (1500 °C; 89.92%td), pores close and adopt a spherical shape, corresponding to the final stage of sintering (Fig. 2d). In conclusion, the pore content decreased during the sintering process and their "elliptical" shape disappeared progressively at high density where it became closed with a spherical shape.

3.2. Thermal properties

The change in heat capacity versus temperature is shown in Fig. 3: up to 500 °C the heat capacity increases with temperature and remains constant above this temperature. This is in good agreement with the literature [28] and this evolution can be modelled by a polynomial fit given by the following equation:

$$c_p = 0.3062 + 6.69 * 10^{-4} * T - 1.34 * 10^{-6} * T^2 + 1.15 * 10^{-9} * T^3 - 3.56 * 10^{-13} * T^4 \quad (20)$$

This polynomial function has a similar behaviour as expected for ceramic oxide materials [24].

The thermal diffusivity of six kinds of samples from 55.67 to 96.32%td are shown in Fig. 4a. Diffusivity decreases logarithmically with temperature and increases with relative density, moreover it increases linearly to the reverse of temperature as theoretically expected (Fig. 4b).

The temperature and porosity dependence of the thermal conductivity up to 1000 °C is shown in Fig. 5. For high porosity content it decreases slowly with temperature and faster for low porosity content. Clearly the thermal conductivity increases with increasing density and decreases with increasing temperature: for example the thermal conductivity decreases from 13 to 3 W/m K for the densest sample (96.32%td) from room temperature up to 1000 °C, as described in the literature [28].

For all samples at room temperature, the thermal conductivity as function of fractional porosity has been fitted to a polynomial

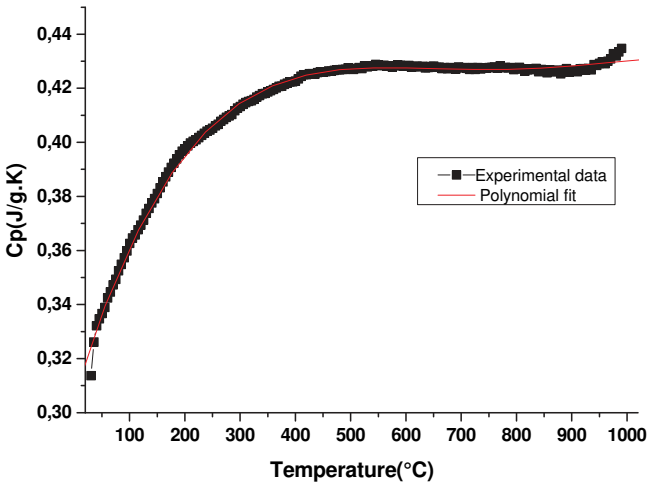

Fig. 3. Heat capacity for the CeO_2 powder in argon.

function (Eq. (21)). The thermal conductivity at full density λ_0 can be determined from this function. It gives for a full dense sample ($p = 0$) λ_0 equal to 15.15 W/m K.

$$\lambda = -160.643p^3 + 45.354p^2 - 7.437p + 15.157 \quad (21)$$

with p as the fractional porosity.

The same methodology was used for determining λ_0 at 500 and 1000 °C. The obtained values are respectively: 6.05 and 2.70 W/m K.

3.3. Dielectric properties

The real and imaginary parts of the dielectric properties are reported in Fig. 6(a and b) in 3D plot in order to show the effect of temperature and porosity on these parameters.

It shows the dielectric properties (real (a) and imaginary (b) parts) from room temperature up to 1000 °C versus the fractional porosity for all prepared samples (from 55.6% to 95.5%td). The relative dielectric constant varies linearly with temperature and is higher for the denser specimens (Fig. 6a). On the other side, the loss factor (or imaginary part of permittivity) does not change significantly below 700 °C, but it becomes very high when the temperature increases (Fig. 6b). Moreover, it becomes higher, when the density was close to the sample which presents high porosity ratio.

The ε'_{eff} increases slowly with temperature and inversely proportional and quickly with porosity (Fig. 6a), ε''_{eff} depends much more on the temperature, especially at high temperature from 750–800 °C (Fig. 6b).

As for thermal conductivity, for all samples at room temperature, the dielectric permittivity (ε') as function of fractional porosity

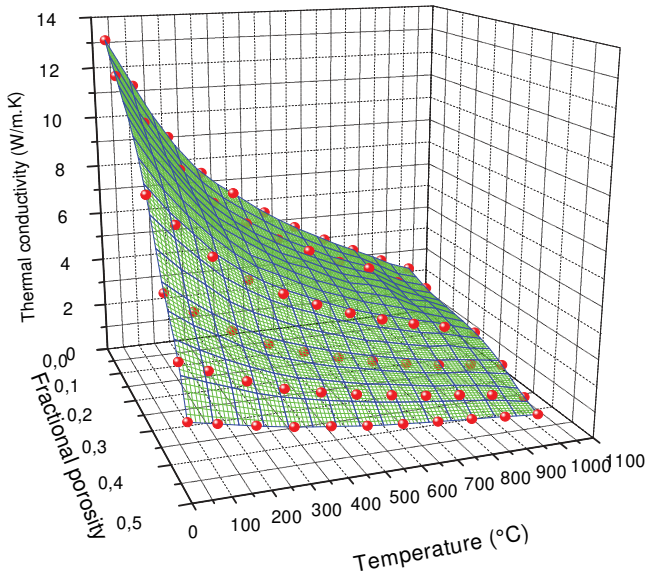

Fig. 5. Variation of the thermal conductivity versus the fractional porosity and temperature.

has been modelized using a polynomial function (Eq. (22)). Its value for full dense sample can be determined from this function. It gives for a full dense sample ($p = 0$) ε'_d equal to 19.55:

$$\varepsilon' = -160.643p^3 + 45.354p^2 - 7.437p + 19.55 \quad (22)$$

with p as the fractional porosity.

4. Discussion

4.1. Effect of the porosity on the thermal conductivity

As we have seen in the results before concerning the thermal conductivity, the contribution of the porosity seems to be more important than the temperature, globally during the heating processing. In fact, for the ceria powder used in this study, sintering starts above 1000 °C, Fig. 5 shows that the thermal conductivity decreases strongly up to low values before the beginning of densification and slightly increases as the sample densifies.

A comparison with Aivazov and Domashnev's model (Eq. (6)) which is well known for low range of porosities, using different values of a parameter at room temperature, are presented in Fig. 7. Here, the experimental data and the theoretical models of the relative thermal conductivity λ/λ_0 for different values of a (0, 1, 10, 15) are presented. According to the model, for lower values of porosity

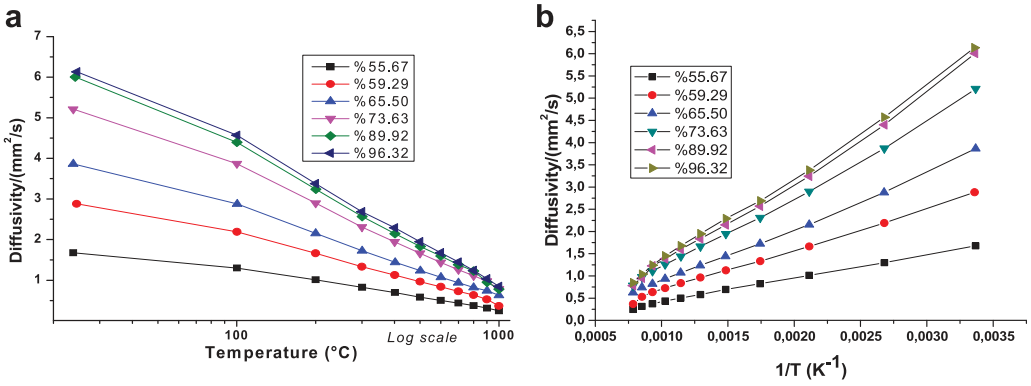

Fig. 4. Variation of the thermal diffusivity (a) versus the temperature and (b) inverse of temperature for 6 different samples (different densities).

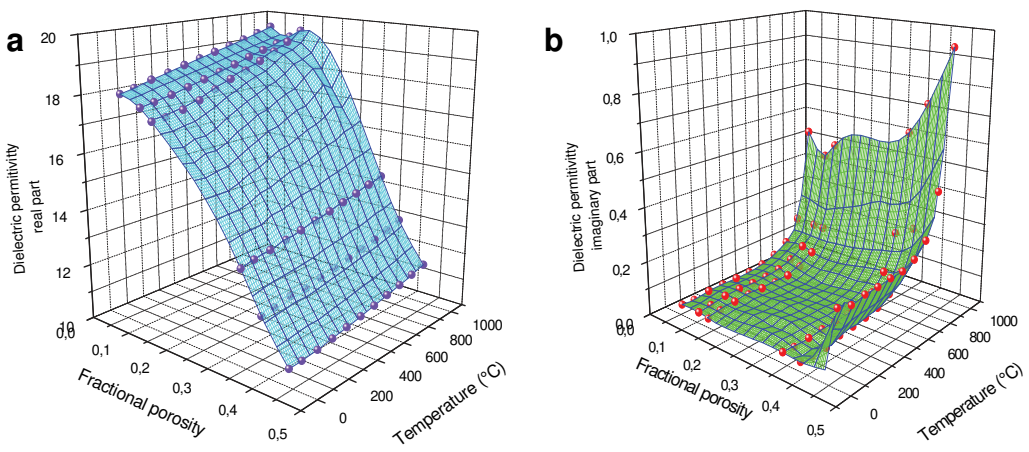

Fig. 6. Variation of the relative dielectric properties (a) real and (b) imaginary parts versus the fractional porosity and the temperature.

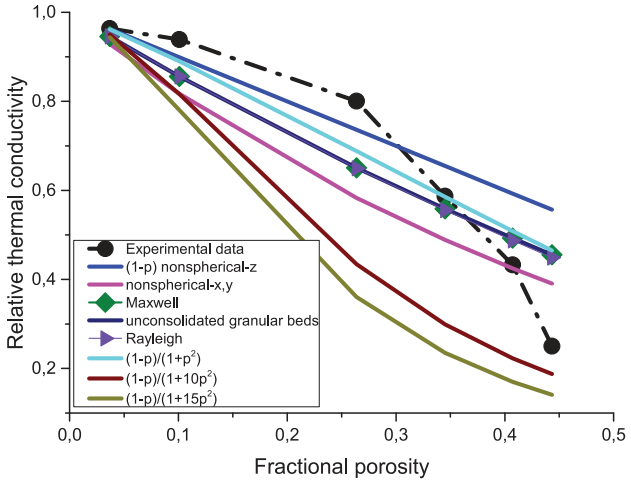

Fig. 7. Variation of the relative thermal conductivity λ/λ_0 versus the fractional porosity at room temperature from our experiments (black) compared with different models from [15–21].

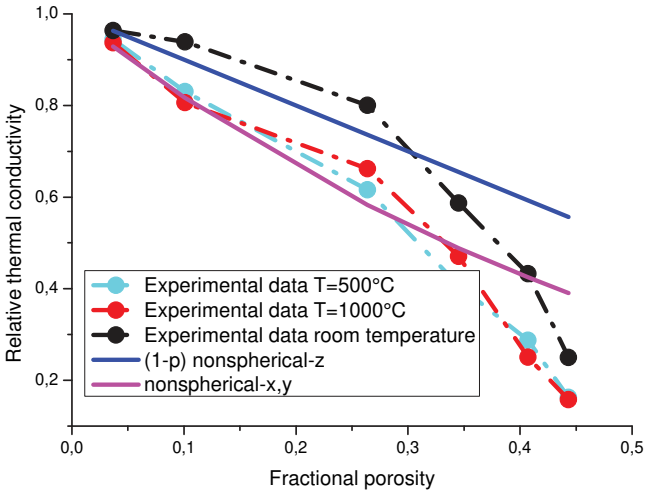

Fig. 8. Variation of the relative thermal conductivity λ/λ_0 versus the fractional porosity at room temperature (black) 500 °C (cyan) and 1000 °C (red) compared with two models. (For interpretation of the references to color in this figure legend, the reader is referred to the web version of this article.)

(less than 0.27), when a parameter increases the model moves from linear variation with very low slope to high slope for high values of a parameter.

Comparing the several models, it appears that the Maxwell's model for spherical inclusions for small volume fraction p and the one for complex inclusions in case of unconsolidated granular beds (with $\alpha \equiv 1{\cdot}5$) are equivalent (Fig. 7). The last both models are very close to Rayleigh's model. Comparing with experiments, the nonspherical-z component (or the linear model $a = 0$) is more suitable at low porosity values less than 0.27. Beyond this value the relative thermal conductivity decreases more rapidly than the various models (Maxwell, Rayleigh, anisotropic components and for high values of a parameter).

At room temperature and high densification (greater than 73%td) the pores appeared with spherical and elliptical shape and the experimental results are closed to the linear model which concerns the porous materials having spherical shape of pores. However, for lower densification the larger pore size and tortuosity depart from the linear model.

Moreover, for high temperature the results at 500 °C and 1000 °C (Fig. 8) show a similar behaviour as at room temperature for all domains of porosity. Comparing to the 2 models presented in Fig. 8, the relative thermal conductivity fits well with the nonspherical x–y model at low values of porosities less than 0.27.

4.2. *Effect of the porosity on the dielectric properties*

Because the real part of the dielectric permittivity is more dependent on the porosity than the temperature, we present in Fig. 9 the comparison of the experimental data at room temperature with Maxwell-Garnet model (Eq. (2)). The values of ε' decrease linearly from 18.24 to 10.5 while the porosity increases from 4.5 up to 43.5 vol%.

In Fig. 9, the upper curve represents the model using 23 as value for the full dense dielectric constant extracted from the literature [29]. And the lowest curve represents the same model using the extrapolated value of ε' at full densification from our experiments 19.55. Therefore, the results are in relative good agreement with model for the full range of porosity.

On the contrary of the thermal conductivity results, the real part of permittivity is not modified by the microstructure evolution observed during the sintering process and especially the change of the shape.

The temperature dependence of the loss factor can be explained by the effect of the ionic conduction of oxygen at elevated temperature. It is known that ceria can modify its stoichiometric composition by reduction the Ce^{4+} to Ce^{3+} accommodating about 14% of oxygen vacancies at 800 °C [30]. The literature shows that the ionic conductivity of ceria has a different behaviour at high

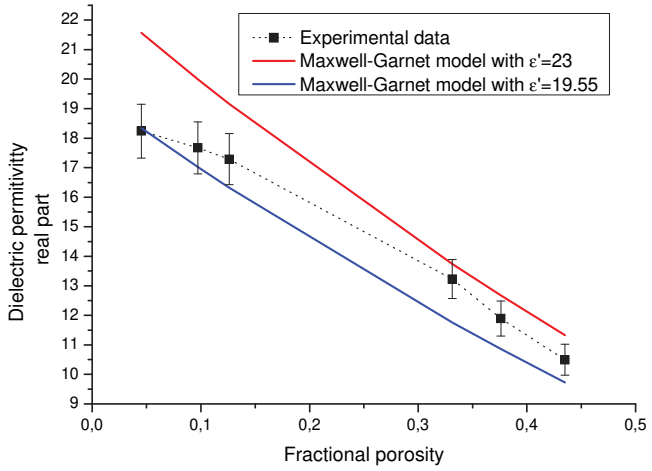

Fig. 9. Variation of the relative dielectric properties (real part) ε' versus the fractional porosity and the Maxwell-Garnet models.

temperature at around 750 °C and this change can explain the big increase (Fig. 6b) of the loss factor at this temperature [31].

5. Conclusion and future works

During the conventional sintering of ceria powder materials, we showed that the microstructure evolved especially the size and the shape and tortuosity of the pores. As a result, the thermal conductivity depends on the porosity and temperature but more on porosity. Moreover, the ratio λ/λ_0 was also affected by the tortuosity of the pores and especially for high fractional porosity (greater than 0.27).

The dielectric properties have been studied up to 1000 °C, the results showed that the loss factor (ε'') depends on the temperature and is strongly affected in porous sample, while the dielectric constant (ε') was more affected by the porosity content than the temperature. Moreover, the pore shapes have no influence on ε' and our results are in good agreement with Maxwell-Garnet model.

In order to enrich both models (Aivazov and Domashnev and Maxwell-Garnett); it will be interesting to take into account not only the pores content but also their shape and tortuosity. For microwave assisted sintering of cerium oxide, heating (which is related to ε'') is independent of the densification excepted for the initial state (the most porous state) of the process. Microwave heating above 750 °C, is possible due to the ionic conduction of ceria, but below this temperature a hybrid heating which combines the conventional and microwave heating is required.

Acknowledgment

The authors thank Dr. Lassi Karvonen and Dr. Sascha Populoh for their assistant in the thermal measurements at EMPA Dübendorf. We thank also the CCEM Project CCEM-Nr 705: Methods of Advanced Waste Treatment (MeAWaT) for the financial support.

References

[1] E. Marani, Microwave applications in neuromorphology and neurochemistry: safety precautions and techniques, Methods 15 (1998) 87–99.
[2] M. Komorowska-Durka, et al., Application of microwave heating to pervaporation: a case study for separation of ethanol–water mixtures, Chem. Eng. Process.: Process Intensif. 81 (2014) 35–40.
[3] O.P. Gandhi, Microwave Engineering and Applications, Pergamon Press, New York, NY, 1981.
[4] S. Chandrasekaran, et al., Microwave food processing—a review, Food Res. Int. 52 (2013) 243–261.
[5] D. Agrawal, et al., Microwave Processing of Ceramics, Composites and Metallic Material, The American Ceramic Society, Ohio, 2005, pp. 205–228.
[6] J.M. Osepchuk, IEEE Trans. Microwave Theory Tech. 32 (1984) 1200–1224.
[7] D.E. Clark, et al., Processing materials with microwave energy, Mater. Sci. Eng., A 287 (2000) 153–158.
[8] S. Logothetidis, et al., Dielectric properties and electronic transitions of porous and nanostructured CeO_2 films, Mater. Sci. Eng., B 109 (2004) 69–73.
[9] H.T. Tuller, A.S. Nowick, Small polaron electron transport in reduced CeO_2 single crystals, J. Phys. Chem. Solids 38 (1977) 859–867.
[10] A.B. Corradi, F. Bondioli, A.M. Ferrari, T. Manfredini, Synthesis and characterization of nanosized ceria powders by microwave–hydrothermal method, Mater. Res. Bull. 41 (1) (2006) 38–44.
[11] M.E. Huntelaar, et al., The thermodynamic properties of Ce_2O_3 (s) from $T = 0$ K to 1500 K, J. Chem. Thermodyn. 32 (2000) 465–482.
[12] M. Cabanes-Sempere, et al., Prog. Nucl. Energy 57 (May) (2012) 111–116.
[13] J.C. Maxwell Garnet, Coulors in metal glasses and in metallic films, Philos. Trans. R. Soc. London 203 (1904) 385–420.
[14] K.W. Schlichting, et al., Thermal conductivity of dense and porous yttria-stabilized zirconia, J. Mater. Sci. 36 (2001) 3003–3010.
[15] J. Francl, W.D. Kingery, Thermal conductivity: IX, Experimental investigation of effect of porosity on thermal conductivity, J. Am. Ceram. Soc. 37 (1954) 99–107.
[16] M.I. Aivazov, IA. Domashnev, Influence of porosity on the conductivity of hot pressed titanium nitride specimens, Poroshk. Metall. 8 (1968) 51–54.
[17] S.K. Rhee, Porosity–thermal conductivity correlations for ceramics materials, Mater. Sci. Eng. 20 (1975) 89–93.
[18] J.C. Maxwell, A Treatise on Electricity and Magnetism, vol. 1, third ed., Oxford University Press, New York, 1891, pp. 314 (reprinted 1998).
[19] J.W. Strutt, Lord Rayleich, Philos. Mag. 34 (5) (1892) 431–502.
[20] V.I. Odelevskii, J. Tech. Phys. (USSR) 24 (1954) 667.
[21] W. Woodside, J.H. Messmer, J. Appl. Phys. 32 (1961) 1688–1706.
[22] Netzsch, Technical, Analyzing and Testing Manual/LFA 457 MicroFlash, Netzsch, 2012.
[23] E. Garcia, et al., Thermal diffusivity of porous cordierite ceramic burners, J. Appl. Phys. 92 (2002) 2346–2349.
[24] "Measuring the dielectric constant of solids with HP8510 network analyzer", August 1985, Hewlett Packard Product Note 8510-3.
[25] D. Kajfez, E.J. Hwan, Q-factor measurement with network analyzer, IEEE Trans. Microwave Theory Tech. 32 (July) (1984) 666–670.
[26] J. Jow, et al., Microwave heating and dielectric diagnosis technique in a single mode resonant cavity, J. AIP 60 (January) (1989) 96–103.
[27] L.F. Chen, et al., Microwave Electronics: Measurement and Materials Characterization, Wiley, England, Nov 2004.
[28] H.Y. Xiao, et al., Thermodynamic properties of $Ce_xTh_{1-x}O_2$ solid solution from first-principles calculations, Acta Mater. 61 (January (2)) (2013) 467–476.
[29] M.T. Sebastian, et al., Microwave dielectric properties of $(1-x)CeO_2$–$xCaTiO_3$ and $(1-x)CeO_2$–xSm_2O_3 ceramics, J. Eur. Ceram. Soc. 24 (2004) 2583–2589.
[30] T. Yamamoto, et al., First-principles study of dielectric properties of cerium oxide, J. Thin Solid Films 486 (2005) 136–140.
[31] H. Yahiro, et al., Oxygen ion conductivity of the ceria–samarium oxide system with fluorite structure, J. Appl. Electrochem. 18 (1988) 527–531.